Macromolecules

pubs.acs.org/Macromolecules Article

RAFT Dispersion Polymerization of Methyl Methacrylate in Mineral Oil: High Glass Transition Temperature of the Core-Forming Block Constrains the Evolution of Copolymer Morphology

Csilla György, Chloe Verity, Thomas J. Neal, Matthew J. Rymaruk, Erik J. Cornel, Timothy Smith, David J. Growney, and Steven P. Armes*

Cite This: https://doi.org/10.1021/acs.macromol.1c01528 Read Online

ACCESS | Metrics & More | Article Recommendations | Supporting Information

ABSTRACT: RAFT dispersion polymerization of a prototypical methacrylic monomer, methyl methacrylate (MMA), is performed in mineral oil using various poly(lauryl methacrylate) (PLMA) precursors prepared with a trithiocarbonate-based RAFT agent. GPC analysis indicated reasonably narrow molecular weight distributions ($M_w/M_n \leq 1.39$) for all diblock copolymers, with ^{1}H NMR studies indicating high MMA conversions (≥95%) for all syntheses. An efficient one-pot synthesis protocol enabled high blocking efficiencies to be achieved when targeting higher PMMA DPs. However, the relatively high glass transition temperature (T_g) of the corresponding core-forming PMMA block unexpectedly constrains the evolution in copolymer morphology during polymerization-induced self-assembly (PISA). More specifically, well-defined $PLMA_{22}$−$PMMA_x$ spheres (x = 19−39) and relatively short worms (x = 69−97) can be obtained at 90 °C when using a $PLMA_{22}$ precursor but targeting higher x values ($x \geq 108$) invariably leads to colloidally unstable aggregates of spheres, rather than long worms or vesicles. Interestingly, similar constraints were observed when targeting higher solids, when using *n*-dodecane instead of mineral oil, or when employing an alternative steric stabilizer block. Raising the PISA synthesis temperature from 90 to 115 °C (i.e., from below to above the T_g of the final PMMA block) does not alleviate this unexpected problem. Moreover, only spherical nanoparticles can be obtained at 115 °C when targeting PMMA DPs between 50 and 400 with the same $PLMA_{22}$ precursor. This suggests that nanoparticle formation may occur by a chain expulsion/insertion mechanism at this relatively high reaction temperature. $PLMA_{22}$−$PMMA_x$ nanoparticles were characterized in terms of their particle size and morphology using dynamic light scattering (DLS), transmission electron microscopy (TEM), and small-angle X-ray scattering (SAXS). DLS and TEM studies of a 0.1% w/w dispersion of $PLMA_{22}$−$PMMA_{69}$ short worms indicated an irreversible worm-to-sphere transition on heating from 20 to 150 °C. Oscillatory rheology and TEM studies indicated that this thermal transition was only partially reversible for a 20% w/w dispersion of $PLMA_{22}$−$PMMA_{69}$ short worms.

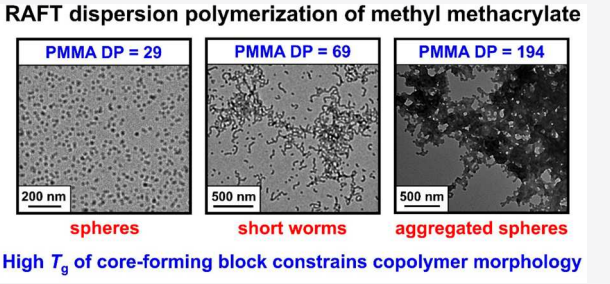

INTRODUCTION

Polymerization-induced self-assembly (PISA) is now well-established as a robust protocol for the convenient synthesis of diblock copolymer nano-objects.[1−6] Typically, reversible addition-fragmentation chain transfer (RAFT) polymerization[7−10] is used to prepare a soluble precursor block. This precursor is then chain-extended using a suitable monomer/solvent pair such that the growing second block becomes insoluble in the reaction mixture once it reaches a certain critical degree of polymerization (DP). This causes micellar nucleation, and the ensuing self-assembly eventually leads to the formation of sterically stabilized diblock copolymer nanoparticles. Notably, very high final monomer conversions can be achieved within short reaction times, and such PISA syntheses can be performed in concentrated solution. Moreover, depending on the relative volume fractions of each block−and providing various other conditions are also fulfilled−the final copolymer morphology can be adjusted to obtain spheres, worms, vesicles, or lamellae.[3−5,11,12]

PISA formulations have been developed for use in aqueous solution,[3,13−17] for polar solvents such as lower alcohols,[18−24] and for non-polar media.[4,25,26] In the latter case, the solvent can be mineral oil[27−35] or silicone oil[36−38] or an *n*-alkane.[39−48] The first two solvents are well-suited for certain potential applications. For example, highly anisotropic worm-like nanoparticles can serve as useful thickeners for silicone oils, particularly if they are rendered stiffer via core cross-linking.[37]

Received: July 20, 2021
Revised: September 20, 2021

Scheme 1. (a) Two-Pot Synthesis Involving the Initial Preparation and Purification of a Poly(lauryl methacrylate) ($PLMA_{22}$) Precursor *via* RAFT Solution Polymerization of LMA in Toluene at 50% w/w Solids Using Methyl 4-Cyano-4-(dodecylthiocarbonothioylthio)pentanoate (MCDP) at 80 °C, Followed by the RAFT Dispersion Polymerization of Methyl Methacrylate (MMA) at 70 °C (Using AIBN), 90 °C (Using T21s) or 115 °C (Using DCP) in Mineral Oil at 20% w/w Solids. (b) One-Pot Synthesis of $PLMA_{19}$−$PMMA_x$ Nanoparticles in Mineral Oil at 20% w/w Solids Using MCDP and T21s at 90 °C[a]

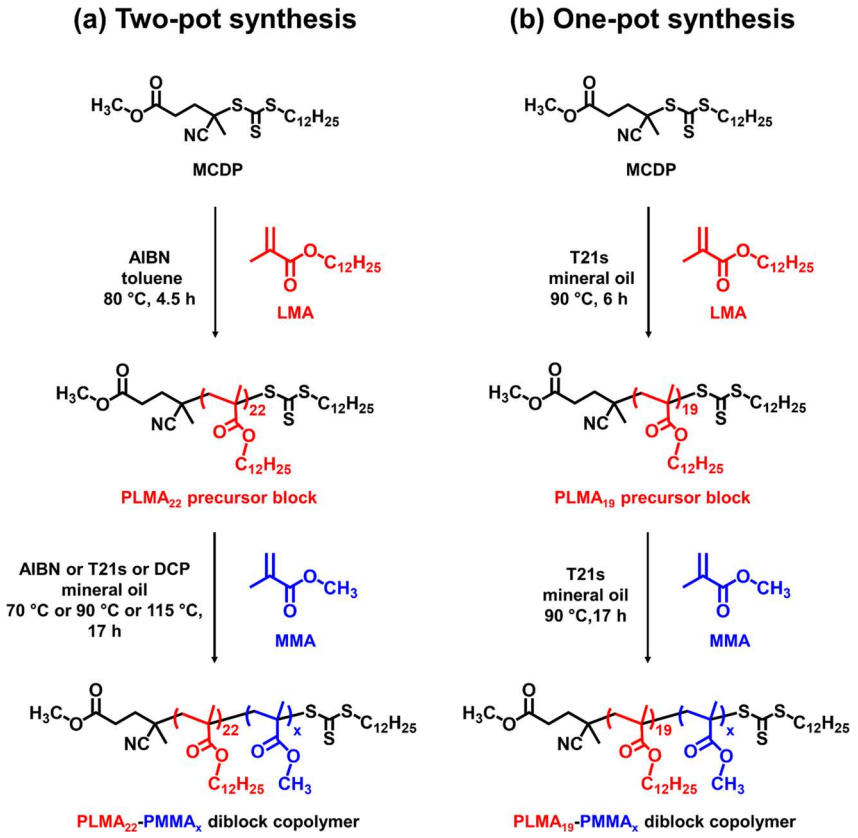

[a]In this case, the $PLMA_{19}$ precursor was chain-extended immediately without further purification after its synthesis at 60% w/w solids. [N.B. AIBN, DCP, and T21s denote 2,2′-azoisobutyronitrile, dicumyl peroxide, and *tert*-butyl peroxy-2-ethylhexanoate initiators, respectively.]

In the case of mineral oil, spherical nanoparticles can act as highly effective lubricants when formulating ultralow viscosity automotive engine oils, which enables greater fuel economy, lower CO_2 emissions, and reduced long-term engine wear to be achieved.[32] However, *n*-alkanes are preferred for fundamental studies, such as the design of model hydrophobic nanoparticles for Pickering (nano)emulsions,[49−58] the development of thermoresponsive nano-objects[29,35,40−42] or highly transparent dispersions that facilitate spectroscopic studies of the fidelity of the organosulfur end-groups during the RAFT polymerization.[45,47]

A wide range of diblock copolymers have been prepared via PISA in non-polar media. The soluble precursor block is typically either poly(lauryl methacrylate)[27,39,40,46] or poly(stearyl methacrylate).[28−34,41−44,47] However, alternative examples include poly(2-ethylhexyl acrylate),[25,26] poly(lauryl acrylate),[48] poly(behenyl methacrylate),[59] or 3-[tris(trimethylsilyloxy)silyl] propyl methacrylate.[38] In addition, monohydroxy-capped precursors such as polydimethylsiloxane[36] or hydrogenated polybutadiene[60,61] can be converted into suitable macromolecular RAFT agents via esterification using a suitable carboxylic acid-functionalized RAFT agent. Similarly, various types of structure-directing insoluble blocks have been studied, including poly(benzyl methacrylate),[27−29,32,38−40] poly(benzyl acrylate),[48] poly(3-phenylpropyl methacrylate),[41−43] poly(glycidyl methacrylate),[30,31] poly(2-hydroxypropyl methacrylate),[34] poly(2,2,2-trifluoroethyl methacrylate),[45,47,62] or poly(2-(dimethylamino)ethyl methacrylate).[36]

Methyl methacrylate (MMA) is the cheapest commodity methacrylic monomer. Indeed, it is often employed as a starting material for the preparation of a range of methacrylic monomers via transesterification with the appropriate alcohol. Herein we explore the RAFT dispersion polymerization of MMA in mineral oil, which is the most cost-effective PISA formulation for the synthesis of methacrylic diblock copolymer nano-objects in non-polar media. A pseudo-phase diagram has been constructed for the preparation of $PLMA_y$−$PMMA_x$ nanoparticles at 20% w/w solids in mineral oil at 90 °C by systematically varying the target DP for the PMMA block from 20 to 200 when using three PLMA precursors of varying DP. Initially, two-pot PISA syntheses were performed, but subsequently a more efficient one-pot protocol was developed (see Scheme 1). To examine the effect of the reaction temperature on the copolymer morphology, these syntheses were not only conducted at 70 and 90 °C (i.e., below the T_g of the PMMA block) but also conducted at 115 °C (i.e., above the T_g of the PMMA block). A series of diblock copolymer nano-objects were also synthesized at 90 °C by (i) varying the solids content, (ii) using *n*-dodecane instead of mineral oil, and

https://doi.org/10.1021/acs.macromol.1c01528
Macromolecules XXXX, XXX, XXX−XXX

(iii) employing an alternative steric stabilizer. The particle size and morphology were characterized using dynamic light scattering (DLS) and transmission electron microscopy (TEM) and, in some cases, by small-angle X-ray scattering (SAXS). Finally, the thermoresponsive behavior of $PLMA_{22}$−$PMMA_{69}$ short worms was briefly studied using DLS, oscillatory rheology, and TEM.

RESULTS AND DISCUSSION

Synthesis of PLMA Precursors for the Two-Pot Synthesis Protocol. PLMA precursors with mean DPs of 22, 30, or 41 were prepared via RAFT solution polymerization of LMA in toluene at 80 °C using MCDP as a RAFT agent (see Scheme 1 and Figure S1). Preliminary kinetic studies of the RAFT solution polymerization of LMA when targeting a $PLMA_{20}$ precursor indicated first-order kinetics after an initial induction period of 1 h and confirmed the linear evolution of molecular weight with conversion (see Figure S2). To avoid the possible loss of RAFT chain-ends under monomer-starved conditions,[45] such polymerizations were quenched after 4.5 h for $PLMA_{22}$ and $PLMA_{30}$, and after 5.5 h for $PLMA_{41}$. ^{1}H NMR studies confirmed relatively high LMA conversions (≥89%) (see Table S1). THF GPC analysis indicated a narrow molecular weight distribution ($M_w/M_n \leq 1.13$) in each case, suggesting that relatively good RAFT control was achieved.

Kinetic Studies of the RAFT Dispersion Polymerization of MMA in Mineral Oil. A representative kinetic experiment was conducted for the RAFT dispersion polymerization of MMA at 90 °C when targeting $PLMA_{19}$−$PMMA_{100}$ nano-objects at 20% w/w solids in mineral oil using the one-pot protocol (see Scheme 1b). The corresponding semi-logarithmic plot indicates two distinct linear regimes (see Figure 1a) as previously reported for various examples of RAFT dispersion polymerization conducted in either aqueous[63] or non-polar media.[27,30,34,36,60] The first regime corresponds to a relatively slow solution polymerization, followed by an approximate ten-fold rate enhancement after 30 min. This corresponds to the onset of micellar nucleation: the growing PMMA block becomes insoluble in the reaction mixture which leads to the *in situ* formation of spherical micelles via self-assembly.[12,36,39] The MMA conversion was 29% at this time point, which corresponds to a critical PMMA DP of 29. Moreover, TEM studies confirm the appearance of nascent spherical nanoparticles in the reaction mixture after 30 min (see Figure 2). DLS studies indicated a *z*-average diameter of 16 nm (DLS polydispersity, PDI = 0.11) for such nuclei (see Figure 2a). Thereafter, first-order kinetics were observed up to 97% MMA conversion, followed by a slower rate of polymerization under monomer-starved conditions. ^{1}H NMR spectroscopy studies indicated that a final MMA conversion of 99% was achieved after 150 min. A linear increase in M_n with conversion and relatively low dispersities ($M_w/M_n \leq 1.14$) were confirmed by THF GPC analysis, see Figure 1b.[7,8,64] This is consistent with the pseudo-living character expected for a well-controlled RAFT polymerization. The final copolymer morphology was a mixture of spheres and short worms (*z*-average diameter = 123 nm, DLS PDI = 0.22), see Figure 2. Similar kinetic studies were also conducted when targeting $PLMA_{22}$−$PMMA_{30}$ spheres using the two-pot protocol at 20% w/w solids in mineral oil, see Figure S3.

GPC Analysis of PLMA−PMMA Diblock Copolymers. PLMA has been previously utilized as a steric stabilizer block by Fielding et al. for the RAFT dispersion polymerization of benzyl methacrylate in non-polar media[27,39,40] More recently, Cornel et al. reported the RAFT dispersion polymerization of MMA using a $PLMA_{39}$ precursor in *n*-dodecane. For this latter PISA formulation, targeting a PMMA DP of either 50 or 100 produced spherical nanoparticles.[46] In each case, GPC analysis indicated narrow molecular weight distributions (M_w/M_n < 1.14), which suggests reasonably good RAFT control. Herein the RAFT dispersion polymerization of MMA was conducted at 20% w/w solids in mineral oil at 90 °C using either a $PLMA_{22}$ precursor block in a two-pot protocol or a $PLMA_{19}$ precursor using a one-pot protocol (see Scheme 1).

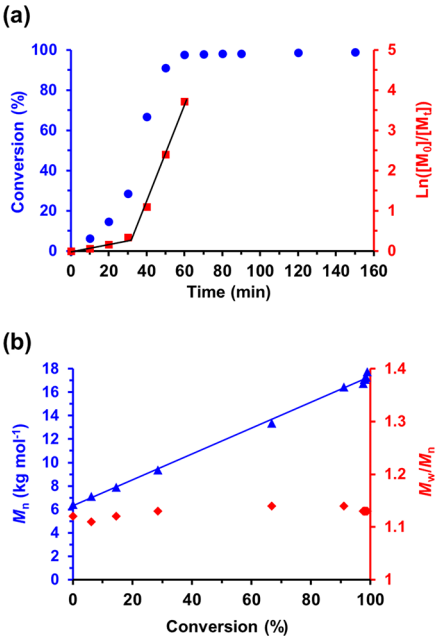

Figure 1. (a) Conversion vs. time curve (blue circles) and corresponding ln([M_0]/[M_t]) vs. time plot (red squares) for the RAFT dispersion polymerization of MMA at 90 °C when targeting $PLMA_{19}$−$PMMA_{100}$ spheres using the one-pot synthesis protocol (see Scheme 1b) at 20% w/w solids in mineral oil. (b) Evolution of M_n (blue triangles) and M_w/M_n (red diamonds) with monomer conversion for this PISA formulation.

Chromatograms recorded for the purified $PLMA_{22}$ precursor and five $PLMA_{22}$−$PMMA_x$ diblock copolymers (where *x* ranges from 19 to 194) prepared using the traditional two-pot protocol are shown in Figure 3a. For comparison, chromatograms obtained for the $PLMA_{19}$ precursor and five $PLMA_{19}$−$PMMA_x$ diblock copolymers (where *x* ranges from 20 to 198) prepared by the one-pot protocol under otherwise identical conditions are shown in Figure 3b. A systematic shift toward higher molecular weight was observed in both cases when targeting higher PMMA DPs. The two-pot protocol resulted in unimodal curves for PMMA DPs of 19, 50, and 97. However, a low molecular weight shoulder became increasingly evident when higher PMMA DPs were targeted. Similar observations were reported by Fielding et al. for the synthesis of $PLMA_{17}$−$PBzMA_x$ nano-objects by the RAFT dispersion polymerization of benzyl methacrylate in *n*-heptane.[39] This feature indicates the presence of unreacted PLMA precursor (or prematurely terminated $PLMA_{22}$−$PMMA_x$ chains). This suboptimal blocking efficiency inevitably leads to broader molecular weight distributions when targeting higher PMMA DPs, *e.g.*, M_w/M_n = 1.16 for $PLMA_{22}$−$PMMA_{97}$ vs. M_w/M_n = 1.36 for $PLMA_{22}$−$PMMA_{194}$.

https://doi.org/10.1021/acs.macromol.1c01528
Macromolecules XXXX, XXX, XXX−XXX

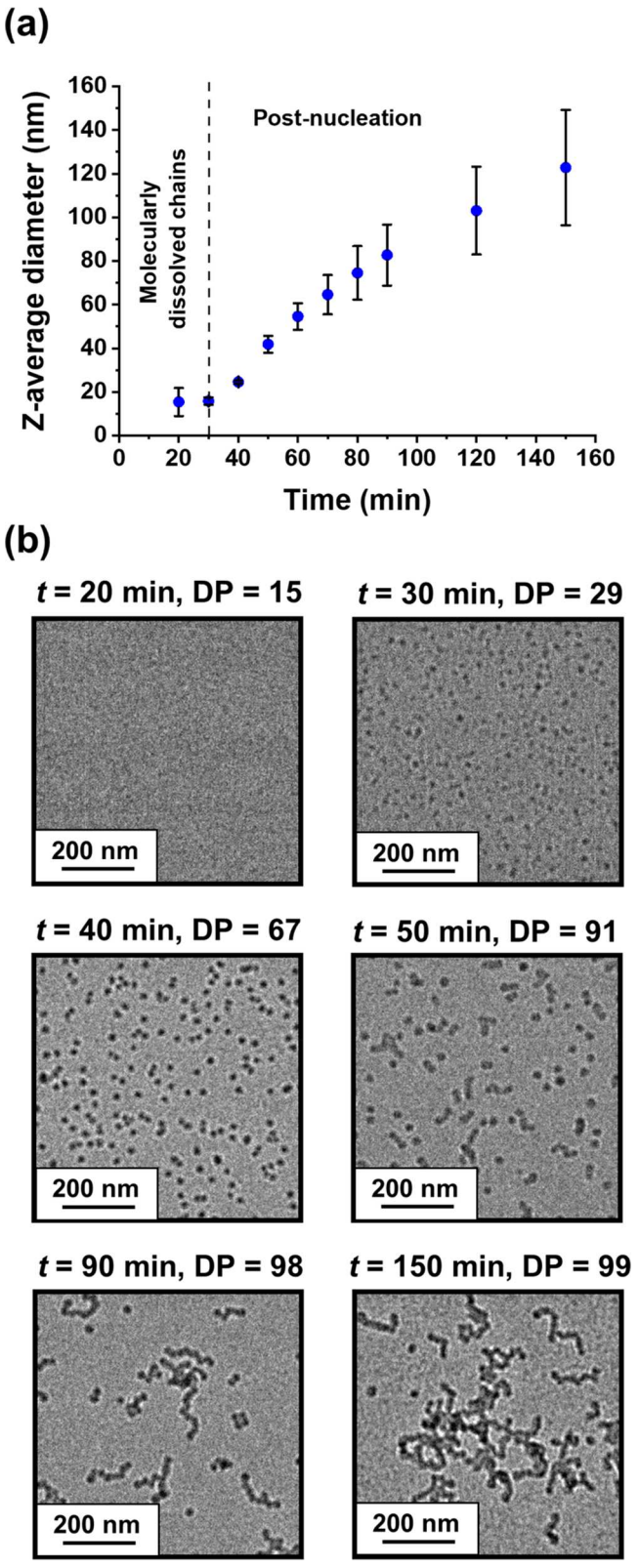

Figure 2. (a) Variation in *z*-average diameter over time obtained for aliquots periodically taken from the reaction mixture when targeting $PLMA_{19}$–$PMMA_{100}$ nano-objects using the one-pot protocol at 90 °C in mineral oil at 20% w/w solids. [N.B. Standard deviations are calculated from the DLS polydispersities and indicate the breadth of each particle size distribution, rather than the experimental error.] (b) Representative TEM images recorded for aliquots taken from the reaction mixture after 20, 30, 40, 50, 90, or 150 min.

In contrast, the one-pot protocol was more efficient (final MMA conversions ≥ 98%; Figure S4) and afforded unimodal chromatograms with significantly narrower MWDs ($M_w/M_n \leq 1.21$) in all cases (see Table S2). In this case, the pseudo-living character of the RAFT dispersion polymerization is enhanced by minimizing the time for which the $PLMA_{19}$ precursor is exposed to monomer-starved conditions at elevated temperature.[45] For both synthesis protocols, a linear relationship was observed between the GPC M_n data and the PMMA DP (corrected for the final MMA conversion), see Figure 3.

Pseudo-phase Diagram Constructed for $PLMA_y$–$PMMA_x$ Nano-objects Prepared in Mineral Oil at 90 °C using the Two-Pot Protocol. A pseudo-phase diagram was constructed for the two-pot synthesis protocol using $PLMA_{22}$, $PLMA_{30}$ and $PLMA_{41}$ precursors by systematically varying the PMMA DP between 20 and 200 (see Tables S3 and S4) while targeting 20% w/w solids in mineral oil at 90 °C. Previous PISA syntheses conducted in non-polar media suggested that employing a sufficiently short steric stabilizer block should provide access to the three main copolymer morphologies (i.e., spheres, worms, and vesicles).[31,34,39,47] In practice, vesicles were not obtained even when using the shortest stabilizer block (see Figure 4). In this case, DLS studies indicated the formation of spheres with *z*-average diameters of 18–30 nm (DLS PDI < 0.20) for PMMA DPs ranging between 19 and 39. Targeting $PLMA_{22}$–$PMMA_{50}$ and $PLMA_{22}$–$PMMA_{59}$ produced viscous liquids comprising mixtures of spheres and short worms. For PMMA DPs ranging between 69 and 97, mainly short worms were obtained with only a minor population of spheres; these dispersions formed transparent, free-standing gels, whereas targeting higher PMMA DPs (≥108) formed turbid brittle gels. Both DLS and TEM studies indicated the formation of micron-sized aggregates of spherical nanoparticles for these latter formulations.

Similar observations were made for a series of $PLMA_{19}$–$PMMA_x$ nano-objects prepared using the one-pot protocol (see Figure S5), suggesting that the synthesis route does not have a significant effect on the copolymer morphology. Well-defined spheres were produced when the $PLMA_{30}$ precursor was chain-extended with MMA. For example, *z*-average diameters of 24–26 nm (DLS PDI ≤ 0.06) were observed for $PLMA_{30}$–$PMMA_{29}$ and $PLMA_{30}$–$PMMA_{49}$. However, targeting higher PMMA DPs only afforded a mixture of spheres and short worms prior to the formation of colloidally unstable aggregates of spherical nanoparticles (e.g., for $PLMA_{30}$–$PMMA_{139}$).

Employing the $PLMA_{41}$ stabilizer only allowed access to kinetically-trapped spheres. Similar morphological limitations have been reported for other PISA formulations in non-polar media.[39,30] In addition to the steric stabilizer DP, there are various other synthesis parameters that may influence the chain mobility of the PMMA block, including the solids content, the solvent composition, and the chemical nature of the steric stabilizer. Interestingly, we observed the same unexpected morphological limitation (i.e., no access to either long worms or vesicles) when targeting a series of $PLMA_{19}$–$PMMA_x$ nanoparticles: (i) at 30% w/w solids in mineral oil, (ii) using *n*-dodecane instead of mineral oil at 20% w/w solids or (iii) when employing poly(stearyl methacrylate) (PSMA) as a steric stabilizer instead of PLMA to target $PSMA_{10}$–$PMMA_{30–200}$ nano-objects in mineral oil at 20% w/w solids (see Figure 5, Table S5, and Table S6).

https://doi.org/10.1021/acs.macromol.1c01528
Macromolecules XXXX, XXX, XXX–XXX

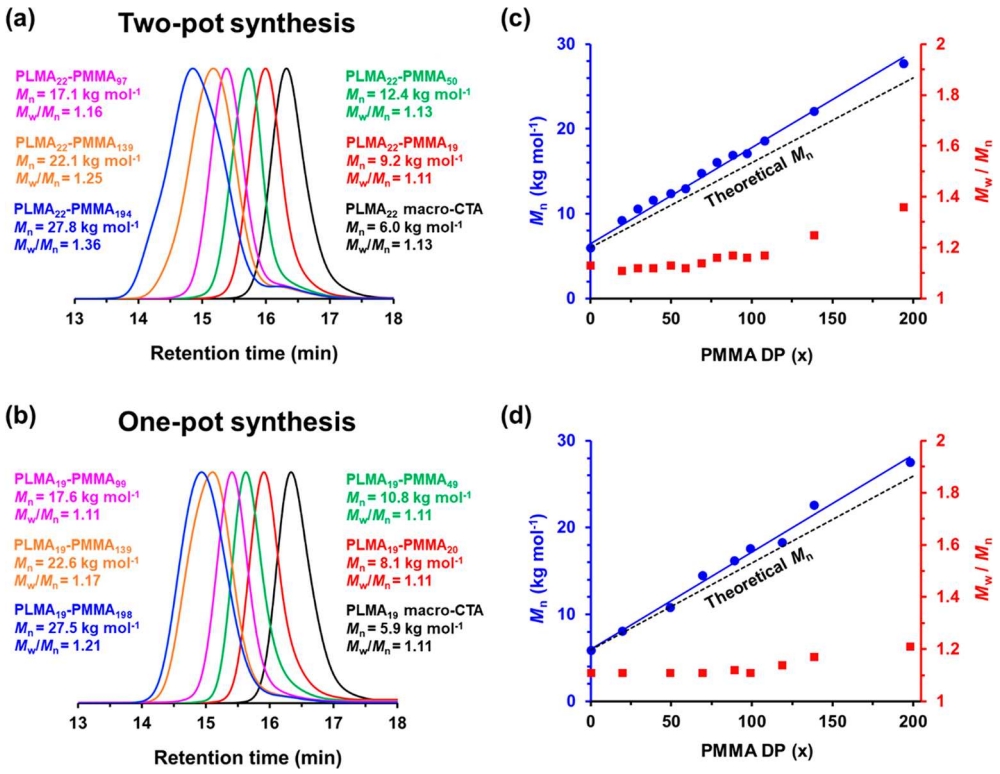

Figure 3. GPC curves (vs a series of near-monodisperse poly(methyl methacrylate) calibration standards using a refractive index detector) recorded for (a) the $PLMA_{22}$ precursor (prepared in toluene at 80 °C targeting 50% w/w solids) and a series of five $PLMA_{22}$−$PMMA_x$ diblock copolymers prepared by RAFT dispersion polymerization of MMA at 90 °C targeting 20% w/w solids using the *two-pot protocol*, where x = 19, 50, 97, 139, or 194, respectively, and (b) the $PLMA_{19}$ precursor (prepared in mineral oil at 90 °C targeting 60% w/w solids) and a series of five $PLMA_{19}$−$PMMA_x$ diblock copolymers prepared using the *one-pot protocol* at 90 °C targeting 20% w/w solids, where x = 20, 49, 99, 139 or 198, respectively. Linear relationship between M_n (blue circles) and PMMA DP (as determined by ^{1}H NMR studies) for a series of (c) $PLMA_{22}$−$PMMA_x$ and (d) $PLMA_{19}$−$PMMA_x$ diblock copolymers prepared at 20% w/w solids. The corresponding M_w/M_n (red squares) data are also shown.

Synthesis of $PLMA_{22}$−$PMMA_x$ Diblock Copolymers above the T_g of the PMMA Block. The unexpected observations described above invite the following question: why does targeting higher PMMA DPs using a $PLMA_{22}$ or $PLMA_{19}$ precursor result in the formation of large spherical aggregates instead of relatively long worms or vesicles? Ideally, PISA should be performed above the effective glass transition temperature of the core-forming block: this is important because it ensures sufficient chain mobility to provide access to higher order morphologies. Conversely, if PISA syntheses are conducted below the T_g of the core-forming block, this is likely to lead to the formation of kinetically-trapped spheres, since the growing solvophobic chains become increasingly stiff and immobile during the polymerization.[65,66]

Therefore, determining the T_g of the core-forming PMMA block is important for understanding the morphological limitations observed herein. The relationship between the T_g and M_n (or DP) for a homopolymer is described by the Flory−Fox equation.[67,68] To determine the molecular weight dependence for the T_g of PMMA, DSC studies were conducted on a series of near-monodisperse PMMA homopolymers with DPs ranging between 13 and 1270 (see Figure S6). For DPs above 200, the T_g is essentially constant at approximately 126 °C, which is in reasonable agreement with the literature value for PMMA.[69−71] As expected, targeting lower DPs leads to a gradual reduction in the T_g below this upper limit value. This is important because the PMMA DPs used to construct the pseudo-phase diagram shown in Figure 4 range from 20 to 200. Thus the PMMA T_g is often significantly lower than the literature value and, in many cases, also below the reaction temperature (90 °C) at which these PISA syntheses are conducted. On the other hand, targeting a PMMA DP of 200 at 90 °C generates chains whose T_g exceeds the reaction temperature. However, literature precedent suggests that the effective T_g of PMMA is likely to be lower when such chains are conjugated to a well-solvated, highly mobile low T_g polymer such as PLMA.[72,73] To examine this hypothesis, four $PLMA_{22}$−$PMMA_x$ diblock copolymers were purified by precipitation to remove residual monomer and solvent and subsequently analyzed by DSC, see Figure 6. It is perhaps worth emphasizing that the T_g of the $PMMA_x$ blocks determined by this method is almost certainly higher than the effective T_g of the growing PMMA chains during PISA. This is because the presence of unreacted MMA monomer within the nanoparticle cores most likely lowers the effective T_g. Bearing in mind this caveat, the T_g for $PLMA_{22}$−$PMMA_{69}$, which comprises mainly short worms, was determined to be 91 °C. This is very close to the reaction temperature, and it may explain why only rather short (as opposed to relatively long) worms could be formed. At intermediate conversions, the growing PMMA chains possess a T_g well below 90 °C and hence are relatively mobile. However, they become increasingly stiff as the MMA polymerization nears completion because (i) the higher PMMA DP leads to a higher T_g and (ii) the lower MMA concentration leads to less plasticization of the PMMA chains. This inevitably reduces the efficiency of the 1D stochastic fusion of multiple spheres that is required to generate the worm morphology.[13,39,40,74] Inspecting Figure 6,

https://doi.org/10.1021/acs.macromol.1c01528
Macromolecules XXXX, XXX, XXX−XXX

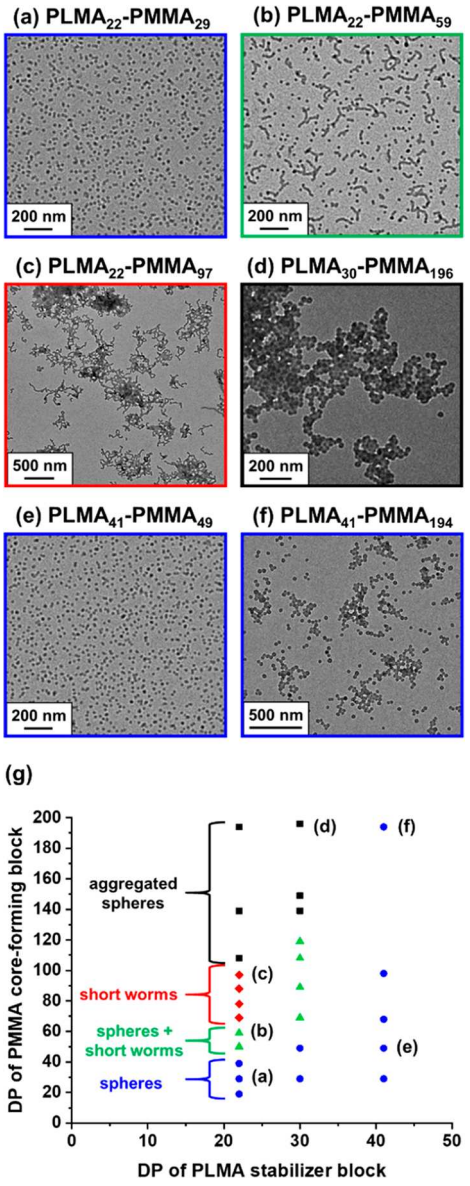

Figure 4. Representative TEM images obtained for (a) $PLMA_{22}$–$PMMA_{29}$ spheres, (b) a mixed phase comprising $PLMA_{22}$–$PMMA_{59}$ spheres and short worms, (c) $PLMA_{22}$–$PMMA_{97}$ short worms, (d) $PLMA_{30}$–$PMMA_{196}$ aggregated spheres, (e) $PLMA_{41}$–$PMMA_{49}$ spheres, and (f) $PLMA_{41}$–$PMMA_{194}$ spheres each prepared at 20% w/w solids in mineral oil, respectively. (g) Pseudo-phase diagram constructed for $PLMA_y$–$PMMA_x$ diblock copolymer nano-objects prepared by RAFT dispersion polymerization of MMA in mineral oil using the two-pot protocol and employing $PLMA_{22}$, $PLMA_{30}$, or $PLMA_{41}$ precursors with T21s initiator at 90 °C ($[PLMA_y]/[T21s]$ molar ratio = 3.0).

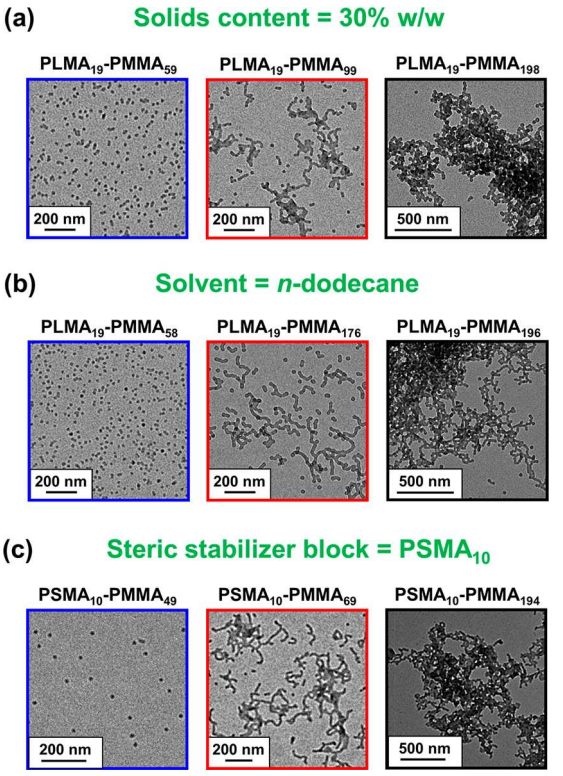

Figure 5. Representative TEM images recorded for (a) $PLMA_{19}$–$PMMA_{59}$, $PLMA_{19}$–$PMMA_{99}$, and $PLMA_{19}$–$PMMA_{198}$ nano-objects prepared at 30% w/w solids in mineral oil using the one-pot protocol; (b) $PLMA_{19}$–$PMMA_{58}$, $PLMA_{19}$–$PMMA_{176}$, and $PLMA_{19}$–$PMMA_{196}$ nano-objects prepared at 20% w/w solids in *n*-dodecane using the one-pot protocol; and (c) $PSMA_{10}$–$PMMA_{49}$, $PSMA_{10}$–$PMMA_{69}$, and $PSMA_{10}$–$PMMA_{194}$ nano-objects prepared at 20% w/w solids in mineral oil with a $PSMA_{10}$ precursor using the two-pot protocol. These images confirm that colloidally unstable aggregates are also obtained for various related formulations, which suggests that this is a generic problem for this PISA system.

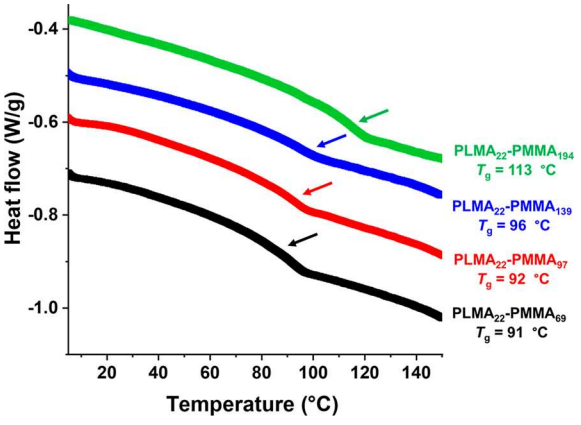

Figure 6. DSC curves recorded for dried $PLMA_{22}$–$PMMA_{69}$, $PLMA_{22}$–$PMMA_{97}$, $PLMA_{22}$–$PMMA_{139}$, and $PLMA_{22}$–$PMMA_{194}$ diblock copolymers (after purification to remove residual monomer and solvent). Clearly, longer PMMA blocks (i.e., higher DPs) lead to higher T_g values.

increasing the PMMA DP from 69 to 194 raises the T_g to approximately 113 °C. According to our PISA synthesis protocol, increasing the target PMMA DP also means a higher MMA concentration within the reaction mixture. Since MMA acts as a co-solvent for the diblock copolymer chains, this delays micellar nucleation until a higher critical PMMA DP is achieved. Presumably, when targeting higher PMMA DPs at 90 °C, the growing chains quickly become too immobile to allow evolution of the copolymer morphology from the spheres that are formed during micellar nucleation. However, one reviewer of this manuscript pointed out that there are various literature reports of aqueous and alcoholic PISA formulations in which nanoparticles with higher order morphologies have been obtained when employing polystyrene as a core-forming block.[75−79] The T_g of polystyrene is comparable to that of

https://doi.org/10.1021/acs.macromol.1c01528
Macromolecules XXXX, XXX, XXX−XXX

PMMA, which suggests that there are likely to be further as-yet-unidentified synthesis parameters that may also influence the evolution in copolymer morphology.

For the present PISA formulation, targeting $x \geq 108$ for $PLMA_{22}$−$PMMA_x$ nano-objects invariably produced colloidally unstable micron-sized aggregates comprising kinetically-trapped spheres (see Figure 4g). Furthermore, DLS studies of a series of $PLMA_{41}$−$PMMA_x$ spheres revealed a linear relationship between the *z*-average diameter and PMMA DPs of 29 to 118 when the data are plotted on a log−log scale (see Figure 7).

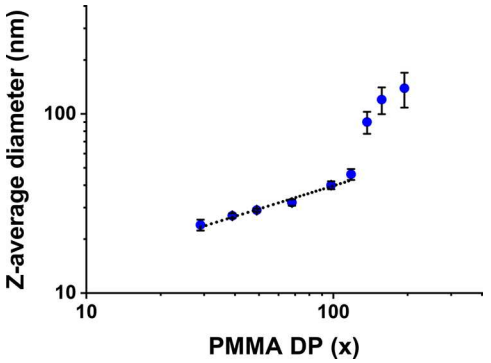

Figure 7. Double logarithmic plot for the relationship between the *z*-average diameter and the PMMA DP (x) for a series of $PLMA_{41}$−$PMMA_x$ (with x ranging from 29 to 194) spheres prepared by RAFT dispersion polymerization of MMA at 90 °C in mineral oil targeting 20% w/w solids using the two-pot protocol. [N.B. Standard deviations are calculated from the DLS polydispersities and thus indicate the breadth of the particle size distributions, rather than the experimental error.]

This enables fine control to be achieved over the particle size over this compositional range. However, the pronounced upturn in apparent particle size indicated by DLS studies suggests incipient nanoparticle flocculation when targeting higher PMMA DPs ($x \geq 137$). This interpretation is consistent with selected TEM images of such nanoparticles shown in Figure 4e and 4f. We are currently unable to explain these unexpected observations. It seems that the longer PLMA chains are unable to confer effective steric stabilization under such conditions. However, this is rather surprising given that significantly higher core-forming block DPs can be targeted for comparable PISA formulations conducted in non-polar media. For example, Derry et al. used a $PLMA_{47}$ precursor to grow core-forming blocks with a mean DP of up to 495 for the RAFT dispersion polymerization of benzyl methacrylate (BzMA) at 90 °C in mineral oil.[27] In this case, well-defined colloidally stable spherical nanoparticles were obtained at up to 50% w/w solids. In closely related work, Derry et al. also used a relatively short poly(stearyl methacrylate) ($PSMA_{31}$) precursor to target a PBzMA DP of up to 2000 in mineral oil.[28] In a follow-up study, Parker and co-workers were able to target PBzMA DPs of up to 3500 using a $PSMA_{54}$ precursor.[33] Similarly, Docherty et al. utilized a $PSMA_{13}$ precursor to grow poly(glycidyl methacrylate) chains with DPs of up to 400 in mineral oil without any loss of colloidal stability for the resulting sterically stabilized spheres.[30] Moreover, the colloidal instability observed in the present study does not seem to be related to the polymerization kinetics. For example, using 2-hydroxypropyl methacrylate (HPMA) leads to a significantly faster rate of RAFT dispersion polymerization compared to less polar methacrylic monomers (e.g., BzMA or MMA), yet PHPMA DPs of up to 150 can be targeted using an oligomeric $PSMA_9$ precursor to generate a vesicular morphology without any loss in colloidal stability.[34] Bearing in mind these prior studies, we conducted a series of PISA syntheses using a longer PSMA block, since this was expected to confer more effective steric stabilization. More specifically, we targeted $PSMA_{37}$−$PMMA_{30-400}$ nano-objects at 20% w/w solids in mineral oil using an alternative trithiocarbonate-based RAFT agent at 90 °C (see Figure S7 and Table S7). Interestingly, DLS studies of these diluted dispersions indicated that colloidally stable spheres were obtained up to a PMMA DP of 100 but only colloidally unstable aggregates were formed when targeting higher DPs. These observations, combined with the results obtained for the series of $PSMA_{10}$−$PMMA_x$ nano-objects (see Figure 5c), suggest that the morphological constraints reported herein are independent of the nature of the steric stabilizer block.

We recently observed that a remarkably similar constraint also applies to the RAFT aqueous emulsion polymerization of MMA at 70 °C.[80] Thus, targeting PMMA DPs up to 80−100 using a non-ionic hydrophilic stabilizer block produced well-defined spheres at 10% w/w solids yet colloidally unstable aggregates were invariably formed when targeting a PMMA DP of 130. This latter observation implies that this phenomenon is likely to be a specific problem associated with the growth of PMMA core-forming blocks below their effective T_g.

Yang et al. reported the PISA synthesis of poly(methacrylic acid)-poly(styrene-*alt*-*N*-phenylmaleimide) diblock copolymer nano-objects in a binary mixture of ethanol and 1,4-dioxane at 70 °C. This reaction temperature is well below the T_g of 219 °C for the core-forming block so vesicles cannot be produced under such conditions. Indeed, this observation was explained in terms of the stiff, inflexible nature of the diblock copolymer chains under the synthesis conditions.[81] Similarly, Wang et al. reported that the copolymer morphology strongly depends on the polymerization temperature for the PISA synthesis of poly(oligo(ethylene oxide) methyl ether methacrylate)-poly(benzyl methacrylate) diblock copolymer nanoparticles in ethanol.[66] More specifically, worms or vesicles could be accessed when the BzMA polymerization was conducted at 65 °C (i.e., above the T_g of the insoluble PBzMA block), whereas only spheres or spherical aggregates could be obtained for syntheses conducted at 25 °C. Similarly, Sobotta et al. examined the synthesis of poly(*N*-acryloylmorpholine)-poly(*N*-acryloylthiomorpholine) (PNAM−PNAT) diblock copolymer nano-objects in aqueous solution. Despite the high T_g of the core-forming PNAT block, the copolymer morphology could be varied from spheres to lamellae when targeting the same diblock copolymer composition ($PNAM_{25}$−$PNAT_{25}$) simply by increasing the synthesis temperature.[82]

In view of this encouraging literature precedent, we decided to examine the PISA synthesis of $PLMA_{22}$−$PMMA_x$ nano-objects above the T_g of PMMA. Since the T_g of the diblock copolymer with the highest PMMA DP ($PLMA_{22}$−$PMMA_{194}$) was 113 °C, we selected the reaction temperature to be 115 °C and chose DCP (whose 10 h half-life is 114 °C) as a suitable initiator. There are two potential technical problems to consider: (i) the thermal stability of the RAFT chain-ends at this elevated temperature and (ii) the potential loss of MMA during the polymerization as its boiling point (101 °C) is below the reaction temperature. For RAFT dispersion

https://doi.org/10.1021/acs.macromol.1c01528
Macromolecules XXXX, XXX, XXX−XXX

polymerizations conducted in non-polar media, our prior studies indicated that trithiocarbonates are much more resistant to thermal degradation than dithiobenzoates.[45,47] Moreover, GPC analysis of diblock copolymers prepared at 115 °C resulted in M_n and M_w/M_n data comparable to those observed for the same diblock composition prepared at 90 °C (see Table S3 and S8). A pseudo-phase diagram was constructed (see Figure 8) to compare the $PLMA_{22}$−$PMMA_x$ nano-objects prepared at 90 °C to those synthesized at 70 and 115 °C, respectively. A similar evolution in morphology from spheres and short worms to colloidally unstable aggregates was observed for PISA syntheses conducted at either 70 or 90 °C. However, targeting the same diblock copolymers at 115 °C merely led to the formation of kinetically-trapped spheres of increasing size when targeting PMMA DPs of 50−400 (see Figure 8a−d). This was a wholly unexpected observation, because selecting this higher temperature was meant to facilitate the evolution in morphology, rather than suppress it.

Recently, Cornel et al. used time-resolved small-angle neutron scattering to demonstrate rapid exchange of individual copolymer chains for a binary mixture of $PLMA_{39}$−$PMMA_{55}$ and $PLMA_{39}$−d_8PMMA_{57} spheres on heating to 150 °C for 3 min.[46] Copolymer chain exchange (which produces hybrid nanoparticle cores comprising both $PMMA_{55}$ and d_8PMMA_{57} blocks) was observed even at 80 °C, which is below the effective T_g for these relatively short core-forming blocks. Given that only spherical nanoparticles were formed during PISA syntheses conducted at 115 °C (Figure 8e), these findings suggest that a chain expulsion/insertion mechanism[46,83−92] most likely occurs under such conditions. In contrast, a micelle fusion/fission mechanism[84,90−92] appears to be favored at either 70 or 90 °C, since such conditions enable the formation of short worms.

SAXS Analysis of PLMA−PMMA Diblock Copolymer Nanoparticles. The pseudo-phase diagrams for $PLMA_y$−$PMMA_x$ nano-objects shown in Figures 4 and 8 were constructed using TEM.[39,93,94] However, this imaging technique invariably suffers from poor statistics. Thus, small-angle X-ray scattering (SAXS) patterns were also recorded for 1.0% w/w dispersions of four examples of $PLMA_{22}$−$PMMA_x$ nano-objects originally synthesized at 20% w/w solids in mineral oil (see Figure 9). SAXS is a statistically reliable technique because X-ray scattering is averaged over millions of particles, whereas TEM studies typically involve the analysis of hundreds of particles. It is well-known that the low q gradient provides morphological information.[95] Thus a zero gradient indicates spherical particles, whereas a gradient of −1 or −2 indicates worms or vesicles, respectively. Data were recorded for $PLMA_{22}$−$PMMA_{29}$ spheres and $PLMA_{22}$−$PMMA_{69}$ short worms prepared at 90 °C and also for $PLMA_{22}$−$PMMA_{114}$ and $PLMA_{22}$−$PMMA_{192}$ spheres synthesized at 115 °C. The low q gradients observed for these four samples (see Figure 9) are consistent with the morphologies assigned by TEM (see Figures 4, 8 and 10). Fitting the SAXS pattern obtained for $PLMA_{22}$−$PMMA_{29}$ using a well-known spherical micelle model[96] indicated an overall diameter (D_{sphere}) of 14.4 ± 2.6 nm with a mean aggregation number (N_{agg}, or number of copolymer chains per nanoparticle) of 190 (see Table S9). Similarly, satisfactory data fits to the SAXS patterns recorded for $PLMA_{22}$−$PMMA_{114}$ and $PLMA_{22}$−$PMMA_{192}$ spheres were obtained using the same spherical model. In the former case, D_{sphere} = 29.2 ± 2.8 nm and N_{agg} = 570, while in the latter case, D_{sphere} = 39.2 ± 4.4 nm and N_{agg} = 900. These volume-average diameters are consistent with the z-average diameters of 36 ± 1.1 nm for $PLMA_{22}$−$PMMA_{114}$ and 50 ± 2.0 nm for $PLMA_{22}$−$PMMA_{192}$ indicated by DLS studies.

Unfortunately, the restricted q range used to record the SAXS pattern for $PLMA_{22}$−$PMMA_{69}$ did not enable precise

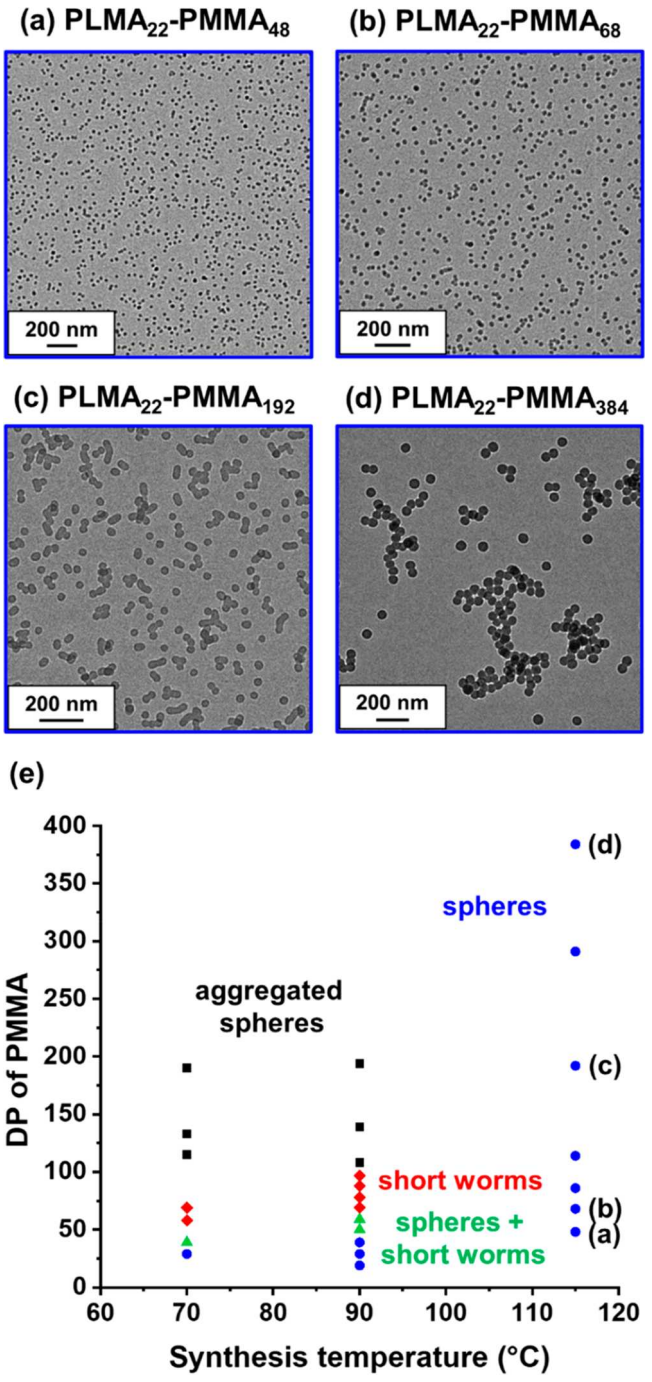

Figure 8. Representative TEM images recorded for the following spherical nanoparticles prepared at 20% w/w solids in mineral oil at 115 °C: (a) $PLMA_{22}$−$PMMA_{48}$, (b) $PLMA_{22}$−$PMMA_{68}$, (c) $PLMA_{22}$−$PMMA_{192}$, and (d) $PLMA_{22}$−$PMMA_{384}$. (e) Pseudo-phase diagram constructed for three series of $PLMA_{22}$−$PMMA_x$ nano-objects prepared by RAFT dispersion polymerization of MMA in mineral oil using the two-pot protocol employing a $PLMA_{22}$ precursor and AIBN initiator at 70 °C, T21s initiator at 90 °C or DCP initiator at 115 °C ([$PLMA_{22}$]/[initiator] molar ratio = 3.0).

https://doi.org/10.1021/acs.macromol.1c01528
Macromolecules XXXX, XXX, XXX−XXX

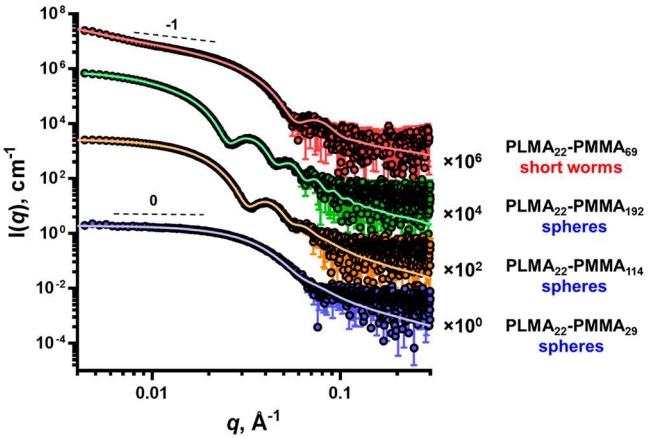

Figure 9. Small-angle X-ray scattering (SAXS) patterns and data fits (solid lines) obtained for 1.0% w/w dispersions of $PLMA_{22}$−$PMMA_{29}$, $PLMA_{22}$−$PMMA_{114}$ and $PLMA_{22}$−$PMMA_{192}$ spheres and $PLMA_{22}$−$PMMA_{69}$ short worms in mineral oil at 20 °C. The $PLMA_{22}$−$PMMA_{29}$ spheres and $PLMA_{22}$−$PMMA_{69}$ short worms were originally prepared at 90 °C at 20% w/w solids in mineral oil using the two-pot protocol while $PLMA_{22}$−$PMMA_{114}$ and $PLMA_{22}$−$PMMA_{192}$ spheres were prepared under the same conditions at 115 °C. Dashed lines indicate gradients of 0 and −1 for guidance.

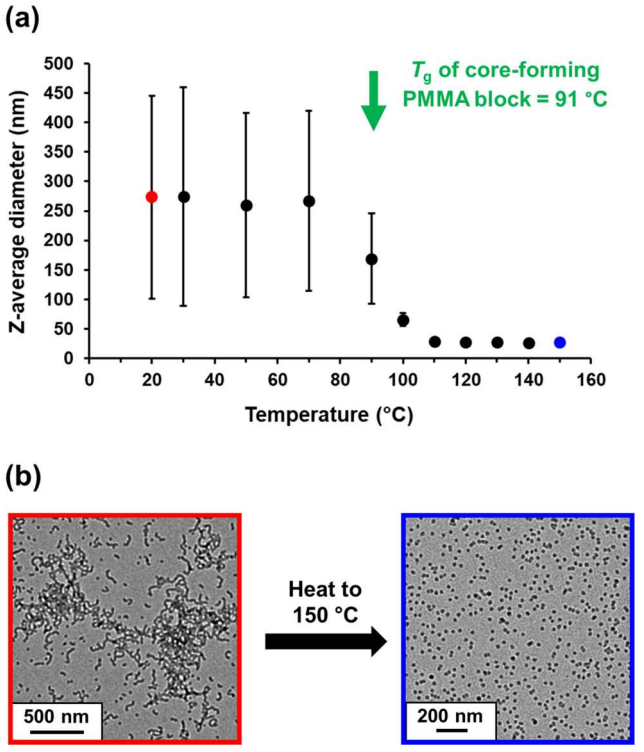

Figure 10. (a) DLS studies showing the variation in apparent hydrodynamic diameter for a 0.1% w/w $PLMA_{22}$−$PMMA_{69}$ dispersion prepared by dilution using *n*-dodecane on heating from 20 to 150 °C [N.B. Standard deviations were calculated from the DLS polydispersity data and indicate the breadth of the particle size distribution, rather than the experimental error.] (b) Representative TEM images obtained for the initial short worms (red frame) and the final spheres that are formed after heating to 150 °C (blue frame).

determination of the worm contour length. However, a satisfactory data fit could be obtained using a worm-like micelle model[96] by fixing the worm contour length at 200 nm (as estimated by TEM analysis). This pragmatic approach indicated an overall cross-sectional worm diameter or worm thickness (T_{worm}) of 14.2 ± 1.4 nm and an N_{agg} of 540.

Thermoresponsive Behavior of $PLMA_{22}$−$PMMA_{69}$ Short Worms. The thermoresponsive behavior of $PLMA_{22}$−$PMMA_{69}$ short worms was examined. This diblock copolymer was selected because this PMMA DP was the lowest for which a soft, free-standing gel was obtained. Moreover, our prior studies suggested that thermally induced morphology transitions were more likely to occur for diblock compositions that lie close to the phase boundary.[29] For DLS analysis, the 20% w/w dispersion of $PLMA_{22}$−$PMMA_{69}$ short worms in mineral oil was diluted to 0.1% w/w using *n*-dodecane. This solvent was preferred as the diluent because it evaporates much faster than mineral oil and does not leave any involatile residues during TEM grid preparation. The resulting dilute dispersion was heated from 20 to 150 °C, with an annealing time of 30 min at each intermediate temperature. An aliquot of this dispersion was extracted at each temperature and cooled to 20 °C prior to DLS measurements. This unusual protocol was adopted because the upper limit temperature for our DLS instrument was only 90 °C, which is insufficient to observe the worm-to-sphere transition for this system. The implicit assumption here is that the dilute nature of the dispersion ensures that the evolving copolymer morphology is always quenched on cooling to 20 °C after each successive thermal annealing step. The initial apparent sphere-equivalent *z*-average diameter was determined to be 273 nm (DLS PDI = 0.63); see Figure 10a. These data are consistent with the polydisperse short worms (plus a minor population of spheres) observed by TEM studies (see Figure 10b). Heating led to a gradual reduction in the apparent hydrodynamic diameter from 267 nm at 70 °C to 169 nm at 90 °C to 66 nm at 100 °C. There is also a significant reduction in the PDI from 0.57 to 0.17 over this temperature range. These observations correlate well with the T_g of the core-forming block, which is 91 °C for $PLMA_{22}$−$PMMA_{69}$. On further heating to 110 °C, a *z*-average diameter of 29 nm and a PDI of 0.05 were observed, which is consistent with the presence of well-defined spherical nanoparticles. Indeed, TEM analysis of the nano-objects formed after thermal equilibration at 150 °C confirmed this morphology, see Figure 10b. Given that this dilute dispersion was cooled to 20 °C prior to DLS analysis, these observations suggest that this thermally-induced morphological transition is essentially irreversible under such conditions. Similar observations were reported by Fielding et al. for a dilute dispersion of $PLMA_{16}$−$PBzMA_{37}$ worms in *n*-dodecane.[40] Clearly, the probability of 1D stochastic fusion of multiple spheres to reform the original short worms is very low at 20 °C, not least because this quenching temperature is well below the T_g of the PMMA block.

The gel comprising $PLMA_{22}$−$PMMA_{69}$ short worms that is formed at 20% w/w solids was characterized by variable temperature oscillatory rheology. This technique has been previously used to study worm-to-sphere[40] and vesicle-to-worm[29,35] transitions for various diblock copolymer systems. The critical gelation temperature (CGT) is indicated by the intersection of the storage modulus (G') and loss modulus (G'') curves and was determined to be 103 °C for the $PLMA_{22}$−$PMMA_{69}$ gel (see Figure 11a). This is consistent with DLS studies, which indicated that only spheres can be obtained above 100 °C (see Figure 10a). Fielding et al. reported a similar rheology study of a $PLMA_{16}$−$PBzMA_{37}$ worm gel prepared in *n*-dodecane.[40] In that case, the

https://doi.org/10.1021/acs.macromol.1c01528
Macromolecules XXXX, XXX, XXX−XXX

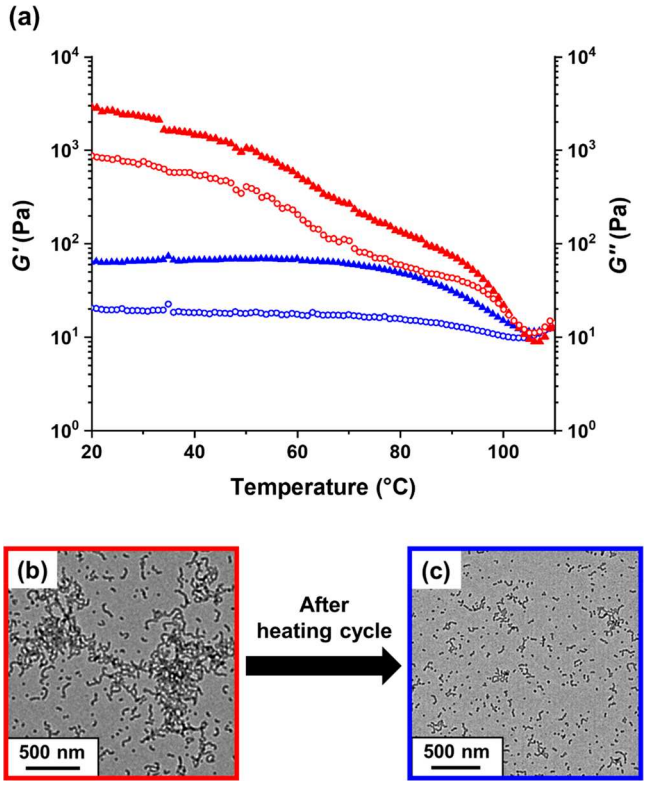

Figure 11. (a) Variation in storage moduli (G', filled triangles) and loss moduli (G'', hollow circles) observed for a 20% w/w dispersion of $PLMA_{22}$–$PMMA_{69}$ short worms in mineral oil on heating from 20 to 110 °C (red symbols) and cooling from 110 to 20 °C (blue symbols) at 2.0 °C min^{-1}. Data were recorded at 1.0% strain amplitude using an angular frequency of 10 rad s^{-1}. Representative TEM images recorded for (b) the initial $PLMA_{22}$–$PMMA_{69}$ short worms and (c) the mixed phase of $PLMA_{22}$–$PMMA_{69}$ short worms and spheres obtained after this oscillatory rheology study.

morphology transition was more or less reversible because the CGT determined during the heating run was close to that observed on cooling. However, the storage modulus for the reconstituted worm gel was reduced from 2300 to 67 Pa, which suggests that significantly shorter worms were formed on the time scale of the experiment. In the present study, intersection of the G' and G'' curves indicated a CGT of approximately 105 °C and the initial and final G' values were 2900 and 65 Pa, respectively. This significant reduction in G' is comparable to that reported by Fielding et al.[40] However, in our case, only a highly viscous fluid was obtained after the thermal cycle instead of a free-standing gel. TEM analysis of the final copolymer dispersion revealed mainly spheres and only a minor population of short worms. Moreover, the mean contour length of the latter nano-objects was significantly shorter than that of the original sample (compare the two TEM images shown in Figure 11). This worm-to-sphere transition is driven via surface plasticization of the worms by ingress of hot solvent. This leads to an increase in the volume fraction of the $PLMA_{22}$ stabilizer block relative to the $PMMA_{69}$ core-forming block, which results in a reduction in the critical packing parameter (P) and thus favors the formation of spheres.[40] It is perhaps noteworthy that the synthesis temperature of 115 °C examined in Figure 8 exceeds the critical gelation temperature (CGT) observed for the 20% w/w dispersion of $PLMA_{22}$–$PMMA_{69}$ nano-objects (see Figure 11). Given that this CGT is associated with a worm-to-sphere transition, this explains why worms cannot be produced at this relatively high temperature: this morphology is simply thermodynamically unstable with respect to spheres under such conditions.

TEM was used to assess the reversibility of the worm-to-sphere transition for the original 20% w/w dispersion of $PLMA_{22}$–$PMMA_{69}$ worms in the absence of applied shear. This worm gel was equilibrated at 150 °C for 1 h, and then a small aliquot was extracted and immediately diluted to 0.1% w/w using hot *n*-dodecane to assess the copolymer morphology. Thereafter, the concentrated dispersion was allowed to cool to 20 °C and then stored at this temperature for 24 h prior to dilution with *n*-dodecane for TEM analysis. Unlike the $PLMA_{16}$–$PBzMA_{37}$ worms reported by Fielding et al.,[40] the original gel was not reformed. Instead, a highly viscous fluid was obtained after this thermal cycle. As shown in Figure S8a, a worm-to-sphere transition was observed on heating but only partial worm reconstitution occurred on cooling to 20 °C. This thermal annealing experiment was repeated but this time the copolymer dispersion was maintained at 90 °C (i.e., around the T_g of the $PMMA_{69}$ chains) for 24 h, instead of simply cooling to 20 °C. However, after aging for a further 24 h at 20 °C, TEM studies indicated an irreversible worm-to-sphere transition in this case (see Figure S8b).

CONCLUSIONS

A series of $PLMA_y$–$PMMA_x$ nano-objects were prepared via RAFT dispersion polymerization of MMA using a $PLMA_{22}$, $PLMA_{30}$ or $PLMA_{41}$ precursor at 90 °C in mineral oil at 20% w/w solids. ^{1}H NMR spectroscopy studies indicated that more than 97% MMA conversion was achieved for such PISA syntheses, while THF GPC confirmed relatively narrow molecular weight distributions ($M_w/M_n \leq 1.39$). An efficient one-pot protocol for the synthesis of $PLMA_{19}$–$PMMA_x$ nano-objects enabled higher blocking efficiencies and narrower molecular weight distributions to be achieved compared to the traditional two-pot protocol using a purified $PLMA_{22}$ precursor. DLS, TEM, and SAXS were used to assess the copolymer morphology. Surprisingly, we were unable to access vesicles, even when using the shortest $PLMA_{22}$ precursor. Instead, only spherical or relatively short worms could be obtained. Moreover, micrometer-sized colloidally unstable aggregates of spheres were invariably produced when targeting higher PMMA DPs (e.g., $PLMA_{22}$–$PMMA_{139}$ or $PLMA_{22}$–$PMMA_{194}$). Such morphological constraints were also observed when performing PISA syntheses (i) at 30% w/w solids in mineral oil, (ii) at 20% w/w solids in *n*-dodecane, or (iii) when employing an alternative steric stabilizer block. The experimental evidence presented herein suggests that these unexpected limitations are related to the high T_g of the core-forming PMMA block. In an attempt to overcome this problem, the synthesis of $PLMA_{22}$–$PMMA_x$ nano-objects was also studied at 115 °C (above the T_g of PMMA). However, only kinetically-trapped spheres were obtained, which suggests that a chain expulsion/insertion mechanism may operate under such conditions. In contrast, the formation of short worms at 70–90 °C suggests a micelle fusion mechanism. Finally, the thermoresponsive behavior of $PLMA_{22}$–$PMMA_{69}$ short worms was assessed by DLS, TEM and oscillatory rheology. A worm-to-sphere transition occurred on heating above 100 °C, which proved to be only partially reversible on cooling. This is consistent with the observation of kinetically-trapped spheres

https://doi.org/10.1021/acs.macromol.1c01528
Macromolecules XXXX, XXX, XXX–XXX

at 115 °C, because short worms are thermodynamically unstable with respect to spheres at this temperature.

■ ASSOCIATED CONTENT

Supporting Information

The Supporting Information is available free of charge at https://pubs.acs.org/doi/10.1021/acs.macromol.1c01528.

Experimental section, assigned ^{1}H NMR spectra for the $PLMA_{22}$ precursor and $PLMA_{19}$−$PMMA_{69}$ diblock copolymers prepared using the one-pot protocol, LMA polymerization kinetics, summary table of PLMA precursors; additional kinetic experiment of targeting $PLMA_{22}$−$PMMA_{30}$ using the two-pot protocol, summary tables of copolymer characterization data, additional TEM images for $PLMA_{19}$−$PMMA_x$ nanoparticles prepared using the one-pot protocol, DSC curves and T_g vs. DP plot for a series of PMMA homopolymers, *z*-average diameter vs. PMMA DP plot for a series of $PSMA_{37}$−$PMMA_x$ spheres plus selected TEM images, summary table for SAXS fitting parameters, and TEM evidence for the partially reversible worm-to-sphere transition exhibited by $PLMA_{22}$−$PMMA_{69}$ worms (PDF)

■ AUTHOR INFORMATION

Corresponding Author

Steven P. Armes − *Dainton Building, Department of Chemistry, University of Sheffield, Sheffield, South Yorkshire S3 7HF, U.K.*; orcid.org/0000-0002-8289-6351; Email: s.p.armes@shef.ac.uk

Authors

Csilla György − *Dainton Building, Department of Chemistry, University of Sheffield, Sheffield, South Yorkshire S3 7HF, U.K.*

Chloe Verity − *Dainton Building, Department of Chemistry, University of Sheffield, Sheffield, South Yorkshire S3 7HF, U.K.*

Thomas J. Neal − *Dainton Building, Department of Chemistry, University of Sheffield, Sheffield, South Yorkshire S3 7HF, U.K.*

Matthew J. Rymaruk − *Dainton Building, Department of Chemistry, University of Sheffield, Sheffield, South Yorkshire S3 7HF, U.K.*

Erik J. Cornel − *Dainton Building, Department of Chemistry, University of Sheffield, Sheffield, South Yorkshire S3 7HF, U.K.*

Timothy Smith − *Lubrizol Ltd., Hazelwood, Derbyshire DE56 4AN, U.K.*

David J. Growney − *Lubrizol Ltd., Hazelwood, Derbyshire DE56 4AN, U.K.*

Complete contact information is available at: https://pubs.acs.org/10.1021/acs.macromol.1c01528

Notes

The authors declare no competing financial interest.

■ ACKNOWLEDGMENTS

We thank the EPSRC for a CDT Ph.D. studentship for C.G. (EP/L016281) and The Lubrizol Corporation Ltd. (Hazelwood, Derbyshire, U.K.) for financial support of this project and for permission to publish these results. S.P.A. also acknowledges an EPSRC *Established Career* Particle Technology Fellowship (EP/R003009). EPSRC is also thanked for a capital equipment grant (EP/J013714) to purchase the Xeuss SAXS instrument. The authors thank Christopher Hill and Dr. Svetomir Tzokov at the University of Sheffield Biomedical Science Electron Microscopy suite.

■ REFERENCES

(1) Charleux, B.; Delaittre, G.; Rieger, J.; D'Agosto, F. Polymerization-Induced Self-Assembly: From Soluble Macromolecules to Block Copolymer Nano-Objects in One Step. *Macromolecules* **2012**, *45*, 6753−6765.

(2) Monteiro, M. J.; Cunningham, M. F. Polymer Nanoparticles via Living Radical Polymerization in Aqueous Dispersions: Design and Applications. *Macromolecules* **2012**, *45*, 4939−4957.

(3) Warren, N. J.; Armes, S. P. Polymerization-Induced Self-Assembly of Block Copolymer Nano-Objects via RAFT Aqueous Dispersion Polymerization. *J. Am. Chem. Soc.* **2014**, *136*, 10174−10185.

(4) Derry, M. J.; Fielding, L. A.; Armes, S. P. Polymerization-Induced Self-Assembly of Block Copolymer Nanoparticles via RAFT Non-Aqueous Dispersion Polymerization. *Prog. Polym. Sci.* **2016**, *52*, 1−18.

(5) Canning, S. L.; Smith, G. N.; Armes, S. P. A Critical Appraisal of RAFT-Mediated Polymerization-Induced Self-Assembly. *Macromolecules* **2016**, *49*, 1985−2001.

(6) Cornel, E. J.; Jiang, J.; Chen, S.; Du, J. Principles and Characteristics of Polymerization-Induced Self-Assembly with Various Polymerization Techniques. *CCS Chem.* **2021**, *3*, 2104−2125.

(7) Chiefari, J.; Chong, Y. K. B.; Ercole, F.; Krstina, J.; Jeffery, J.; Le, T. P. T.; Mayadunne, R. T. A.; Meijs, G. F.; Moad, C. L.; Moad, G.; Rizzardo, E.; Thang, S. H. Living Free-Radical Polymerization by Reversible Addition-Fragmentation Chain Transfer: The RAFT Process. *Macromolecules* **1998**, *31*, 5559−5562.

(8) Moad, G.; Rizzardo, E.; Thang, S. H. Living Radical Polymerization by the RAFT Process. *Aust. J. Chem.* **2005**, *58*, 379−410.

(9) Moad, G.; Rizzardo, E.; Thang, S. H. Toward Living Radical Polymerization. *Acc. Chem. Res.* **2008**, *41*, 1133−1142.

(10) Perrier, S. 50th Anniversary Perspective: RAFT Polymerization - A User Guide. *Macromolecules* **2017**, *50*, 7433−7447.

(11) Penfold, N. J. W.; Yeow, J.; Boyer, C.; Armes, S. P. Emerging Trends in Polymerization-Induced Self-Assembly. *ACS Macro Lett.* **2019**, *8*, 1029−1054.

(12) D'Agosto, F.; Rieger, J.; Lansalot, M. RAFT-Mediated Polymerization-Induced Self-Assembly. *Angew. Chem., Int. Ed.* **2020**, *59*, 8368−8392.

(13) Blanazs, A.; Madsen, J.; Battaglia, G.; Ryan, A. J.; Armes, S. P. Mechanistic Insights for Block Copolymer Morphologies: How Do Worms Form Vesicles? *J. Am. Chem. Soc.* **2011**, *133*, 16581−16587.

(14) Boissé, S.; Rieger, J.; Belal, K.; Di-Cicco, A.; Beaunier, P.; Li, M. H.; Charleux, B. Amphiphilic Block Copolymer Nano-Fibers via RAFT-Mediated Polymerization in Aqueous Dispersed System. *Chem. Commun.* **2010**, *46*, 1950−1952.

(15) Zhang, X.; Boissé, S.; Zhang, W.; Beaunier, P.; D'Agosto, F.; Rieger, J.; Charleux, B. Well-Defined Amphiphilic Block Copolymers and Nano-Objects Formed in Situ via RAFT-Mediated Aqueous Emulsion Polymerization. *Macromolecules* **2011**, *44*, 4149−4158.

(16) Sugihara, S.; Ma'Radzi, A. H.; Ida, S.; Irie, S.; Kikukawa, T.; Maeda, Y. In Situ Nano-Objects via RAFT Aqueous Dispersion Polymerization of 2-Methoxyethyl Acrylate Using Poly(Ethylene Oxide) Macromolecular Chain Transfer Agent as Steric Stabilizer. *Polymer* **2015**, *76*, 17−24.

(17) Figg, C. A.; Carmean, R. N.; Bentz, K. C.; Mukherjee, S.; Savin, D. A.; Sumerlin, B. S. Tuning Hydrophobicity To Program Block Copolymer Assemblies from the Inside Out. *Macromolecules* **2017**, *50*, 935−943.

(18) Lowe, A. B. RAFT Alcoholic Dispersion Polymerization with Polymerization-Induced Self-Assembly. *Polymer* **2016**, *106*, 161−181.
(19) Wan, W. M.; Pan, C. Y. One-Pot Synthesis of Polymeric Nanomaterials via RAFT Dispersion Polymerization Induced Self-Assembly and Re-Organization. *Polym. Chem.* **2010**, *1*, 1475−1484.
(20) Pei, Y.; Lowe, A. B. Polymerization-Induced Self-Assembly: Ethanolic RAFT Dispersion Polymerization of 2-Phenylethyl Methacrylate. *Polym. Chem.* **2014**, *5*, 2342−2351.
(21) Zehm, D.; Ratcliffe, L. P. D.; Armes, S. P. Synthesis of Diblock Copolymer Nanoparticles via RAFT Alcoholic Dispersion Polymerization: Effect of Block Copolymer Composition, Molecular Weight, Copolymer Concentration, and Solvent Type on the Final Particle Morphology. *Macromolecules* **2013**, *46*, 128−139.
(22) Wan, W. M.; Sun, X. L.; Pan, C. Y. Formation of Vesicular Morphologies via Polymerization Induced Self-Assembly and Re-Organization. *Macromol. Rapid Commun.* **2010**, *31*, 399−404.
(23) Semsarilar, M.; Jones, E. R.; Blanazs, A.; Armes, S. P. Efficient Synthesis of Sterically-Stabilized Nano-Objects via RAFT Dispersion Polymerization of Benzyl Methacrylate in Alcoholic Media. *Adv. Mater.* **2012**, *24*, 3378−3382.
(24) Jones, E. R.; Semsarilar, M.; Blanazs, A.; Armes, S. P. Efficient Synthesis of Amine-Functional Diblock Copolymer Nanoparticles via RAFT Dispersion Polymerization of Benzyl Methacrylate in Alcoholic Media. *Macromolecules* **2012**, *45*, 5091−5098.
(25) Houillot, L.; Bui, C.; Save, M.; Charleux, B.; Farcet, C.; Moire, C.; Raust, J. A.; Rodriguez, I. Synthesis of Well-Defined Polyacrylate Particle Dispersions in Organic Medium Using Simultaneous RAFT Polymerization and Self-Assembly of Block Copolymers. A Strong Influence of the Selected Thiocarbonylthio Chain Transfer Agent. *Macromolecules* **2007**, *40*, 6500−6509.
(26) Houillot, L.; Bui, C.; Farcet, C.; Moire, C.; Raust, J. A.; Pasch, H.; Save, M.; Charleux, B. Dispersion Polymerization of Methyl Acrylate in Nonpolar Solvent Stabilized by Block Copolymers Formed in Situ via the RAFT Process. *ACS Appl. Mater. Interfaces* **2010**, *2*, 434−442.
(27) Derry, M. J.; Fielding, L. A.; Armes, S. P. Industrially-Relevant Polymerization-Induced Self-Assembly Formulations in Non-Polar Solvents: RAFT Dispersion Polymerization of Benzyl Methacrylate. *Polym. Chem.* **2015**, *6*, 3054−3062.
(28) Derry, M. J.; Fielding, L. A.; Warren, N. J.; Mable, C. J.; Smith, A. J.; Mykhaylyk, O. O.; Armes, S. P. In Situ Small-Angle X-Ray Scattering Studies of Sterically-Stabilized Diblock Copolymer Nanoparticles Formed during Polymerization-Induced Self-Assembly in Non-Polar Media. *Chem. Sci.* **2016**, *7*, 5078−5090.
(29) Derry, M. J.; Mykhaylyk, O. O.; Armes, S. P. A Vesicle-to-Worm Transition Provides a New High-Temperature Oil Thickening Mechanism. *Angew. Chem., Int. Ed.* **2017**, *56*, 1746−1750.
(30) Docherty, P. J.; Derry, M. J.; Armes, S. P. RAFT Dispersion Polymerization of Glycidyl Methacrylate for the Synthesis of Epoxy-Functional Block Copolymer Nanoparticles in Mineral Oil. *Polym. Chem.* **2019**, *10*, 603−611.
(31) Docherty, P. J.; Girou, C.; Derry, M. J.; Armes, S. P. Epoxy-Functional Diblock Copolymer Spheres, Worms and Vesicles via Polymerization-Induced Self-Assembly in Mineral Oil. *Polym. Chem.* **2020**, *11*, 3332−3339.
(32) Derry, M. J.; Smith, T.; O'Hora, P. S.; Armes, S. P. Block Copolymer Nanoparticles Prepared via Polymerization-Induced Self-Assembly Provide Excellent Boundary Lubrication Performance for Next-Generation Ultralow-Viscosity Automotive Engine Oils. *ACS Appl. Mater. Interfaces* **2019**, *11*, 33364−33369.
(33) Parker, B. R.; Derry, M. J.; Ning, Y.; Armes, S. P. Exploring the Upper Size Limit for Sterically Stabilized Diblock Copolymer Nanoparticles Prepared by Polymerization-Induced Self-Assembly in Non-Polar Media. *Langmuir* **2020**, *36*, 3730−3736.
(34) György, C.; Hunter, S. J.; Girou, C.; Derry, M. J.; Armes, S. P. Synthesis of Poly(Stearyl Methacrylate)-Poly(2-Hydroxypropyl Methacrylate) Diblock Copolymer Nanoparticles via RAFT Dispersion Polymerization of 2-Hydroxypropyl Methacrylate in Mineral Oil. *Polym. Chem.* **2020**, *11*, 4579−4590.
(35) Dorsman, I. R.; Derry, M. J.; Cunningham, V. J.; Brown, S. L.; Williams, C. N.; Armes, S. P. Tuning the Vesicle-to-Worm Transition for Thermoresponsive Block Copolymer Vesicles Prepared: Via Polymerisation-Induced Self-Assembly. *Polym. Chem.* **2021**, *12*, 1224−1235.
(36) Rymaruk, M. J.; Hunter, S. J.; O'Brien, C. T.; Brown, S. L.; Williams, C. N.; Armes, S. P. RAFT Dispersion Polymerization in Silicone Oil. *Macromolecules* **2019**, *52*, 2822−2832.
(37) Rymaruk, M. J.; O'Brien, C. T.; Brown, S. L.; Williams, C. N.; Armes, S. P. Effect of Core Cross-Linking on the Physical Properties of Poly(Dimethylsiloxane)-Based Diblock Copolymer Worms Prepared in Silicone Oil. *Macromolecules* **2019**, *52*, 6849−6860.
(38) Rymaruk, M. J.; O'Brien, C. T.; Brown, S. L.; Williams, C. N.; Armes, S. P. RAFT Dispersion Polymerization of Benzyl Methacrylate in Silicone Oil Using a Silicone-Based Methacrylic Stabilizer Provides Convenient Access to Spheres, Worms, and Vesicles. *Macromolecules* **2020**, *53*, 1785−1794.
(39) Fielding, L. A.; Derry, M. J.; Ladmiral, V.; Rosselgong, J.; Rodrigues, A. M.; Ratcliffe, L. P. D.; Sugihara, S.; Armes, S. P. RAFT Dispersion Polymerization in Non-Polar Solvents: Facile Production of Block Copolymer Spheres, Worms and Vesicles in n-Alkanes. *Chem. Sci.* **2013**, *4*, 2081−2087.
(40) Fielding, L. A.; Lane, J. A.; Derry, M. J.; Mykhaylyk, O. O.; Armes, S. P. Thermo-Responsive Diblock Copolymer Worm Gels in Non-Polar Solvents. *J. Am. Chem. Soc.* **2014**, *136*, 5790−5798.
(41) Pei, Y.; Sugita, O. R.; Thurairajah, L.; Lowe, A. B. Synthesis of Poly(Stearyl Methacrylate-b-3- Phenylpropyl Methacrylate) Nanoparticles in n-Octane and Associated Thermoreversible Polymorphism. *RSC Adv.* **2015**, *5*, 17636−17646.
(42) Pei, Y.; Thurairajah, L.; Sugita, O. R.; Lowe, A. B. RAFT Dispersion Polymerization in Nonpolar Media: Polymerization of 3-Phenylpropyl Methacrylate in N-Tetradecane with Poly(Stearyl Methacrylate) Homopolymers as Macro Chain Transfer Agents. *Macromolecules* **2015**, *48*, 236−244.
(43) Pei, Y.; Noy, J. M.; Roth, P. J.; Lowe, A. B. Soft Matter Nanoparticles with Reactive Coronal Pentafluorophenyl Methacrylate Residues via Non-Polar RAFT Dispersion Polymerization and Polymerization-Induced Self-Assembly. *J. Polym. Sci., Part A: Polym. Chem.* **2015**, *53*, 2326−2335.
(44) Cunningham, V. J.; Armes, S. P.; Musa, O. M. Synthesis, Characterisation and Pickering Emulsifier Performance of Poly-(Stearyl Methacrylate)-Poly(N-2-(Methacryloyloxy)Ethyl Pyrrolidone) Diblock Copolymer Nano-Objects via RAFT Dispersion Polymerisation in n-Dodecane. *Polym. Chem.* **2016**, *7*, 1882−1891.
(45) Cornel, E. J.; Van Meurs, S.; Smith, T.; O'Hora, P. S.; Armes, S. P. In Situ Spectroscopic Studies of Highly Transparent Nanoparticle Dispersions Enable Assessment of Trithiocarbonate Chain-End Fidelity during RAFT Dispersion Polymerization in Nonpolar Media. *J. Am. Chem. Soc.* **2018**, *140*, 12980−12988.
(46) Cornel, E. J.; Smith, G. N.; Rogers, S. E.; Hallett, J. E.; Growney, D. J.; Smith, T.; O'Hora, P. S.; Van Meurs, S.; Mykhaylyk, O. O.; Armes, S. P. Time-Resolved Small-Angle Neutron Scattering Studies of the Thermally-Induced Exchange of Copolymer Chains between Spherical Diblock Copolymer Nanoparticles Prepared: Via Polymerization-Induced Self-Assembly. *Soft Matter* **2020**, *16*, 3657−3668.
(47) György, C.; Derry, M. J.; Cornel, E. J.; Armes, S. P. Synthesis of Highly Transparent Diblock Copolymer Vesicles via RAFT Dispersion Polymerization of 2,2,2-Trifluoroethyl Methacrylate in N-Alkanes. *Macromolecules* **2021**, *54*, 1159−1169.
(48) Ratcliffe, L. P. D.; McKenzie, B. E.; Le Bouëdec, G. M. D.; Williams, C. N.; Brown, S. L.; Armes, S. P. Polymerization-Induced Self-Assembly of All-Acrylic Diblock Copolymers via RAFT Dispersion Polymerization in Alkanes. *Macromolecules* **2015**, *48*, 8594−8607.
(49) Hunter, S. J.; Armes, S. P. Pickering Emulsifiers Based on Block Copolymer Nanoparticles Prepared by Polymerization-Induced Self-Assembly. *Langmuir* **2020**, *36*, 15463−15484.

https://doi.org/10.1021/acs.macromol.1c01528
Macromolecules XXXX, XXX, XXX−XXX

(50) Thompson, K. L.; Mable, C. J.; Cockram, A.; Warren, N. J.; Cunningham, V. J.; Jones, E. R.; Verber, R.; Armes, S. P. Are Block Copolymer Worms More Effective Pickering Emulsifiers than Block Copolymer Spheres? *Soft Matter* **2014**, *10*, 8615−8626.
(51) Thompson, K. L.; Derry, M. J.; Hatton, F. L.; Armes, S. P. Long-Term Stability of n-Alkane-in-Water Pickering Nanoemulsions: Effect of Aqueous Solubility of Droplet Phase on Ostwald Ripening. *Langmuir* **2018**, *34*, 9289−9297.
(52) Thompson, K. L.; Fielding, L. A.; Mykhaylyk, O. O.; Lane, J. A.; Derry, M. J.; Armes, S. P. Vermicious Thermo-Responsive Pickering Emulsifiers. *Chem. Sci.* **2015**, *6*, 4207−4214.
(53) Thompson, K. L.; Lane, J. A.; Derry, M. J.; Armes, S. P. Non-Aqueous Isorefractive Pickering Emulsions. *Langmuir* **2015**, *31*, 4373−4376.
(54) Thompson, K. L.; Mable, C. J.; Lane, J. A.; Derry, M. J.; Fielding, L. A.; Armes, S. P. Preparation of Pickering Double Emulsions Using Block Copolymer Worms. *Langmuir* **2015**, *31*, 4137−4144.
(55) Mable, C. J.; Warren, N. J.; Thompson, K. L.; Mykhaylyk, O. O.; Armes, S. P. Framboidal ABC Triblock Copolymer Vesicles: A New Class of Efficient Pickering Emulsifie. *Chem. Sci.* **2015**, *6*, 6179−6188.
(56) Thompson, K. L.; Cinotti, N.; Jones, E. R.; Mable, C. J.; Fowler, P. W.; Armes, S. P. Bespoke Diblock Copolymer Nanoparticles Enable the Production of Relatively Stable Oil-in-Water Pickering Nanoemulsions. *Langmuir* **2017**, *33*, 12616−12623.
(57) Rymaruk, M. J.; Thompson, K. L.; Derry, M. J.; Warren, N. J.; Ratcliffe, L. P. D.; Williams, C. N.; Brown, S. L.; Armes, S. P. Bespoke Contrast-Matched Diblock Copolymer Nanoparticles Enable the Rational Design of Highly Transparent Pickering Double Emulsions. *Nanoscale* **2016**, *8*, 14497−14506.
(58) Hunter, S. J.; Thompson, K. L.; Lovett, J. R.; Hatton, F. L.; Derry, M. J.; Lindsay, C.; Taylor, P.; Armes, S. P. Synthesis, Characterization, and Pickering Emulsifier Performance of Anisotropic Cross-Linked Block Copolymer Worms: Effect of Aspect Ratio on Emulsion Stability in the Presence of Surfactant. *Langmuir* **2019**, *35*, 254−265.
(59) Derry, M. J.; Mykhaylyk, O. O.; Ryan, A. J.; Armes, S. P. Thermoreversible Crystallization-Driven Aggregation of Diblock Copolymer Nanoparticles in Mineral Oil. *Chem. Sci.* **2018**, *9*, 4071−4082.
(60) Darmau, B.; Rymaruk, M. J.; Warren, N. J.; Bening, R.; Armes, S. P. RAFT Dispersion Polymerization of Benzyl Methacrylate in Non-Polar Media Using Hydrogenated Polybutadiene as a Steric Stabilizer Block. *Polym. Chem.* **2020**, *11*, 7533−7541.
(61) Rymaruk, M. J.; O'Brien, C. T.; György, C.; Darmau, B.; Jennings, J.; Mykhaylyk, O. O.; Armes, S. P. Small-Angle X-Ray Scattering Studies of Block Copolymer Nano-Objects: Formation of Ordered Phases in Concentrated Solution During Polymerization-Induced Self-Assembly. *Angew. Chem., Int. Ed.* **2021**, *60*, 12955−12963.
(62) Smith, G. N.; Derry, M. J.; Hallett, J. E.; Lovett, J. R.; Mykhaylyk, O. O.; Neal, T. J.; Prévost, S.; Armes, S. P. Refractive Index Matched, Nearly Hard Polymer Colloids. *Proc. R. Soc. London, Ser. A* **2019**, *475*, 20180763.
(63) Cunningham, V. J.; Derry, M. J.; Fielding, L. A.; Musa, O. M.; Armes, S. P. RAFT Aqueous Dispersion Polymerization of N-(2-(Methacryloyloxy)Ethyl)Pyrrolidone: A Convenient Low Viscosity Route to High Molecular Weight Water-Soluble Copolymers. *Macromolecules* **2016**, *49*, 4520−4533.
(64) Moad, G.; Rizzardo, E.; Thang, S. H. Radical Addition-Fragmentation Chemistry in Polymer Synthesis. *Polymer* **2008**, *49*, 1079−1131.
(65) Zhou, J.; Zhang, W.; Hong, C.; Pan, C. Promotion of Morphology Transition of Di-Block Copolymer Nano-Objects: Via RAFT Dispersion Copolymerization. *Polym. Chem.* **2016**, *7*, 3259−3267.
(66) Wang, G.; Schmitt, M.; Wang, Z.; Lee, B.; Pan, X.; Fu, L.; Yan, J.; Li, S.; Xie, G.; Bockstaller, M. R.; Matyjaszewski, K. Polymerization-Induced Self-Assembly (PISA) Using ICAR ATRP at Low Catalyst Concentration. *Macromolecules* **2016**, *49*, 8605−8615.
(67) Fox, T. G.; Flory, P. J. Second-Order Transition Temperatures and Related Properties of Polystyrene. I. Influence of Molecular Weight. *J. Appl. Phys.* **1950**, *21*, 581−591.
(68) Fox, T. G.; Flory, P. J. The Glass Temperature and Related Properties of Poly-Styrene. Influence of Molecular Weight. *J. Polym. Sci.* **1954**, *14*, 315−319.
(69) Faivre, A.; David, L.; Vassoille, R.; Vigier, G.; Etienne, S.; Geissler, E. Electronic Density Fluctuations in Disordered Systems. 1. Effect of Thermal Treatments on the Dynamics and Local Microstructure of Poly(Methyl Methacrylate). *Macromolecules* **1996**, *29*, 8387−8390.
(70) Porter, C. E.; Blum, F. D. Thermal Characterization of PMMA Thin Films Using Modulated Differential Scanning Calorimetry. *Macromolecules* **2000**, *33*, 7016−7020.
(71) Brandrup, J.; Immergut, E. H.; McDowell, W. *Polymer Handbook*, 2nd ed.; Wiley: New York, 1975.
(72) Lejars, M.; Margaillan, A.; Bressy, C. Well-Defined Graft Copolymers of Tert-Butyldimethylsilyl Methacrylate and Poly(Dimethylsiloxane) Macromonomers Synthesized by RAFT Polymerization. *Polym. Chem.* **2013**, *4*, 3282−3292.
(73) Wang, W. W.; Jiang, L.; Ren, W. Y.; Zhang, C. M.; Man, C. Z.; Nguyen, T. P.; Dan, Y. The Crystallinity, Thermal Properties and Microscopic Morphology of Di-Block Copolymers of l-Lactide and Several Acrylates. *RSC Adv.* **2016**, *6*, 31934−31946.
(74) Zhang, X.; Rieger, J.; Charleux, B. Effect of the Solvent Composition on the Morphology of Nano-Objects Synthesized via RAFT Polymerization of Benzyl Methacrylate in Dispersed Systems. *Polym. Chem.* **2012**, *3*, 1502−1509.
(75) Pham, B. T. T.; Nguyen, D.; Huynh, V. T.; Pan, E. H.; Shirodkar-Robinson, B.; Carey, M.; Serelis, A. K.; Warr, G. G.; Davey, T.; Such, C. H.; Hawkett, B. S. Aqueous Polymeric Hollow Particles as an Opacifier by Emulsion Polymerization Using Macro-RAFT Amphiphiles. *Langmuir* **2018**, *34*, 4255−4263.
(76) Rieger, J.; Zhang, W.; Stoffelbach, F.; Charleux, B. Surfactant-Free RAFT Emulsion Polymerization Using Poly(N,N -Dimethylacrylamide) Trithiocarbonate Macromolecular Chain Transfer Agents. *Macromolecules* **2010**, *43*, 6302−6310.
(77) Huang, C. Q.; Pan, C. Y. Direct Preparation of Vesicles from One-Pot RAFT Dispersion Polymerization. *Polymer* **2010**, *51*, 5115−5121.
(78) He, W. D.; Sun, X. L.; Wan, W. M.; Pan, C. Y. Multiple Morphologies of PAA-b-PSt Assemblies throughout RAFT Dispersion Polymerization of Styrene with PAA Macro-CTA. *Macromolecules* **2011**, *44*, 3358−3365.
(79) Wan, W. M.; Sun, X. L.; Pan, C. Y. Morphology Transition in RAFT Polymerization for Formation of Vesicular Morphologies in One Pot. *Macromolecules* **2009**, *42*, 4950−4952.
(80) Chan, D. H. H.; Cockram, A. A.; Gibson, R. R.; Kynaston, E. L.; Lindsay, C.; Taylor, P.; Armes, S. P. RAFT Aqueous Emulsion Polymerization of Methyl Methacrylate: Observation of Unexpected Constraints When Employing a Non-Ionic Steric Stabilizer Block. *Polym. Chem.* **2021**, DOI: 10.1039/d1py01008e.
(81) Yang, P.; Ratcliffe, L. P. D.; Armes, S. P. Article Pubs. Acs. Org/Macromolecules Efficient Synthesis of Poly(Methacrylic Acid)-Block-Poly(Styrene-Alt-N-phenylmaleimide) Diblock Copolymer Lamellae Using RAFT Dispersion Polymerization. *Macromolecules* **2013**, *46*, 8545−8556.
(82) Sobotta, F. H.; Kuchenbrod, M.; Hoeppener, S.; Brendel, J. C. One Polymer Composition, Various Morphologies: The Decisive Influence of Conditions on the Polymerization-Induced Self-Assembly (PISA) of N-Acryloyl Thiomorpholine. *Nanoscale* **2020**, *12*, 20171−20176.
(83) Choi, S. H.; Lodge, T. P.; Bates, F. S. Mechanism of Molecular Exchange in Diblock Copolymer Micelles: Hypersensitivity to Core Chain Length. *Phys. Rev. Lett.* **2010**, *104*, 047802.
(84) Cornel, E. J.; O'Hora, P. S.; Smith, T.; Growney, D. J.; Mykhaylyk, O. O.; Armes, S. P. SAXS Studies of the Thermally-

https://doi.org/10.1021/acs.macromol.1c01528
Macromolecules XXXX, XXX, XXX−XXX

Induced Fusion of Diblock Copolymer Spheres: Formation of Hybrid Nanoparticles of Intermediate Size and Shape. *Chem. Sci.* **2020**, *11*, 4312−4321.
(85) Choi, S. H.; Bates, F. S.; Lodge, T. P. Molecular Exchange in Ordered Diblock Copolymer Micelles. *Macromolecules* **2011**, *44*, 3594−3604.
(86) Lu, J.; Bates, F. S.; Lodge, T. P. Remarkable Effect of Molecular Architecture on Chain Exchange in Triblock Copolymer Micelles. *Macromolecules* **2015**, *48*, 2667−2676.
(87) Zhao, D.; Ma, Y.; Lodge, T. P. Exchange Kinetics for a Single Block Copolymer in Micelles of Two Different Sizes. *Macromolecules* **2018**, *51*, 2312−2320.
(88) Zinn, T.; Willner, L.; Pipich, V.; Richter, D.; Lund, R. Molecular Exchange Kinetics of Micelles: Corona Chain Length Dependence. *ACS Macro Lett.* **2016**, *5*, 884−888.
(89) Wang, Y.; Kausch, C. M.; Chun, M.; Quirk, R. P.; Mattice, W. L. Exchange of Chains between Micelles of Labeled Polystyrene-Block-Poly(Oxyethylene) As Monitored by Nonradiative Singlet Energy Transfer. *Macromolecules* **1995**, *28*, 904−911.
(90) Haliloğlu, T.; Bahar, I.; Erman, B.; Mattice, W. L. Mechanisms of the Exchange of Diblock Copolymers between Micelles at Dynamic Equilibrium. *Macromolecules* **1996**, *29*, 4764−4771.
(91) Dormidontova, E. E. Micellization Kinetics in Block Copolymer Solutions: Scaling Model. *Macromolecules* **1999**, *32*, 7630−7644.
(92) Halperin, A.; Alexander, S. Polymeric Micelles: Their Relaxation Kinetics. *Macromolecules* **1989**, *22*, 2403−2412.
(93) Blanazs, A.; Ryan, A. J.; Armes, S. P. Predictive Phase Diagrams for RAFT Aqueous Dispersion Polymerization: Effect of Block Copolymer Composition, Molecular Weight, and Copolymer Concentration. *Macromolecules* **2012**, *45*, 5099−5107.
(94) Warren, N. J.; Mykhaylyk, O. O.; Mahmood, D.; Ryan, A. J.; Armes, S. P. RAFT Aqueous Dispersion Polymerization Yields Poly(Ethylene Glycol)-Based Diblock Copolymer Nano-Objects with Predictable Single Phase Morphologies. *J. Am. Chem. Soc.* **2014**, *136*, 1023−1033.
(95) Glatter, O.; Kratky, O. *Small-Angle X-Ray Scattering*; Academic Press: London, 1982.
(96) Pedersen, J. S. Form Factors of Block Copolymer Micelles with Spherical, Ellipsoidal and Cylindrical Cores. *J. Appl. Crystallogr.* **2000**, *33*, 637−640.

https://doi.org/10.1021/acs.macromol.1c01528
Macromolecules XXXX, XXX, XXX−XXX